Oleg P. Posnansky[1,2] iD

[1]BIF-IZKF, RWTH Aachen University, Aachen, Germany
[2]MPI-HCBS, Leipzig, Germany
e-mail: opoznans@gmail.com

Influence of weak molecular velocity autocorrelation
on the diffusion NMR

Abstract. Self-diffusion of spin-bearing molecules measured by magnetic resonance can noninvasively probe the microstructure of complex soft matter and serve as a powerful tool for different types of diagnostics. Theoretical methods are needed to determine the autocorrelation of molecular velocities and magnetic resonance signal characteristics related to the shape, size, and concentration of soft matter constituents, although their development represents a difficult inverse problem. In this paper, we propose a numerical renormalization method that provides understanding of the contrast diffusion mechanism closely related to both the component hierarchy and the dynamic of molecular motion with a weak correlation with underlying structure. We demonstrate simulations of our method on a heterogeneous material with a self-similar random organization and show that we derive efficient temporal diffusion properties for disordered geometry, size and concentration of its components at different Euclidean dimensions. The proposed approach provides a tool for interpretation of experimental data obtained for meta- and native materials.

Key words: magnetic resonance, signal attenuation, temporal diffusion.

Introduction

Diffusion-weighted nuclear magnetic resonance (NMR) probes the mobility of water spin-bearing molecules and provides high sensitivity to complex compartmentalized media at scales well below spatial resolution. Since the introduction of diffusion-weighted MR, it has become a common method for finding vague differences between composite materials and plays an important role in classifying and forecasting physical properties as influenced by microstructure. MR signal of widespread pulsed field gradient spin echo (PGSE) experiments [1] typically represent the average diffusivity reflecting the concentration and size of components of heterogeneous structures. Correct explanation of diffusion MR data should take into account mesoscopic effects acting from microscopic to macroscopic length scales [2-5]. These effects range from an apparent elemental impact on water mobility, such as the fraction of inhomogeneities, to ensemble actions of partial volume configurations of different inclusion types and angular dispersion. The exchange rate between compartments or multiple relaxation times can also affect the signal, depending on the data collection window of the experiment. Customizing measurement data to identify relationships between a number of parameters allows us to find valuable information content in a sample and can be a method of increasing the specificity of MR signatures. The parametric relationships of these materials are typically featured by distinct nonlinearities, which are particularly pronounced near the percolation (i.e. structural) threshold [6, 7]. A series of classic percolation theory approaches are founded on random impedance networks [8, 9] and have been extensively employed to examine transport behaviour [9-11] and relaxation [12] in disordered composites. Fluctuations of local magnetic fields responsible for measured diffusion and relaxation [12], as well as radio-frequency absorption of magnetic fields [13, 14], have been considered in the random network model. The corresponding models indicate a second-order phase transition and hierarchical features of the magnetic field distributions.

In this paper, we suggest employing the renormalisation group method in a conjunction with MR to achieve a unified description of the temporal fast limiting and spectral diffusion in random

composites, which are commonly utilized as a model to understand the physical characteristics of the of meta- and intrinsically disordered materials [15,16].

The theory of renormalization groups has found numerous applications in various fields of physics, such as in the physics of magnetism [17,18], the description of the conductivity of disordered channels [19-22], coherent ideal absorbers [23], and the mechanical properties of chaotic soft matter [24,25]. On the one hand, each of the above problems has some important symmetries of its own, which lead to different classes of statistical ensembles. On the other hand, they have in common the self-similarity at different scales. Such a hierarchy greatly simplifies the mathematical description of the processes, preserving the influence of the disorder of the constituent elements as a key factor.

First, we describe the attenuation of the MR signal due to diffusion of spin-bearing molecules. The magnitude of the attenuation depends on the waveform of the magnetic field gradient and the velocity autocorrelation of molecules. The analytical extension of the dynamical velocity correlation allows us to apply the perturbation framework to characterize and define the decelerating motion taking into account only weak nonlinearity. Then, in the next section, we construct a hierarchical model of the random composite. The results of numerical simulation of the diffusion MR signal of the composite based on the renormalisation group method are reviewed in the last part and will be summarized and discussed.

Local MR signal attenuation due to diffusion and weak velocity autocorrelation.

Consider an inhomogeneous environment in the in the presence of a constant magnetic field, B_0. If a gradient of the external magnetic field, $G(t)$, is imposed, the random and time-dependent location of the spin bearing particles modulates the spin phase [26]. The resulting spin echo attenuation, $M(t)$, involves correlation between particle velocities [27] and leads to exponential decay:

$$M(t) = e^{-\alpha(t)}, \quad (1)$$

if we assume the Gaussian approximation of spin-phase modulation, characterised by the diffusion

coefficient, D. Note that Eq.(1) is demodulated at the Larmor frequency, $\omega_0 = \gamma B_0$.

The attenuation factor, $\alpha(t)$, in Eq.(1) is

$$\alpha(t) = \frac{\gamma^2}{2} \int_0^t \int_0^t G(t_1) \langle r(t_1) r(t_2) \rangle G(t_2) dt_1 dt_2, \quad (2)$$

where

$$\langle r(t_1) r(t_2) \rangle = \frac{D}{\pi} \int_{-\infty}^{\infty} \langle u(\omega) u^*(\omega) \rangle e^{i\omega(t_1 - t_2)} d\omega,$$

γ is the gyromagnetic ratio, and $\langle u(\omega) u^*(\omega) \rangle$ is the velocity autocorrelation function ($u^*(\omega)$ is a complex-conjugation) after the Fourier transform [27,28] with:

$$u(\omega) = \tau \left(\pi \delta(\omega) - \frac{i\omega\tau}{1 + (\omega\tau)^2} \right) \quad (3a)$$

and

$$u(\omega) u^*(\omega) \big|_{1/\tau \to 0} \approx \tau^2 \left(\pi^2 \delta(\omega) + \frac{1}{2 + (\omega\tau)^2} \right) \quad (3b)$$

if only second order terms of small parameter $1/\tau$ in Eq.(3b) are considered. In Eq. (3) τ indicates the characteristic correlation time, which models the propagation of water molecules in the environment, symbol $\delta(\omega)$ defines Dirac delta-function, and imaginary unit $i = \sqrt{-1}$. In the presence of a static magnetic field, internal heterogeneity can be imitated by changing the magnetic susceptibility along the structure of the soft matter. These background changes of magnetic field are characterized by internal gradients, $G_s(t)$, with amplitude g_s, and might generate measurable effects on MR signal [32]. In this case external gradients, $G(t)$, should be substituted to $G(t) + G_s(t)$ in Eqs.(1,2) taking magnetic susceptibility of complex structures (see Appendix for details) into account. In our further theoretical derivations, we assume $G(t) >> G_s(t)$

providing only effects related to molecular fast-motion.

More strictly, the extent of weak autocorrelation is given by the inequality $\omega\tau \gg 1$ in Eq.(3). Parameter τ describes the interaction with the background medium very coarsely and without differentiating the main types of medium. In addition, as a limitation of the model could be considered the isotropic description of the problem, which is violated in many substances.

A typical diffusion-weighted PGSE sequence has time-varying external magnetic field gradients, $G(t)$, with amplitude g and width δ separated by diffusion time Δ (Fig.1a).
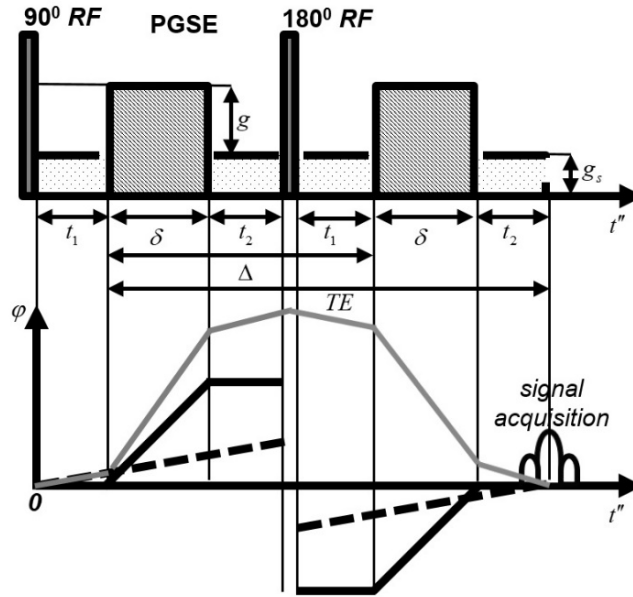
Figure 1.a – Schematic of a diffusion-weighted PGSE sequence with 90º *RF* magnetic field excitation pulse starting at a time $t_0 = 0$ and 180º *RF* magnetic field spin refocusing pulse. *TE* determines the maximum signal during acquisition. External time-varying two-lobe magnetic field gradients are characterized with amplitude g, width δ and separated by diffusion time Δ. Constant background gradients are depicted by amplitude g_s. The bottom part of the plot represents the evolution of the absolute spin phase, φ, during PGSE (gray solid line) if both external and background gradients are present. Separate evolution of the spin phase for the external (solid black line) and internal (dashed black line) gradients is also given. In the absence of external gradients, dephasing occurs due to the background spatial change in the magnetic field (dashed line).

The spins are excited by radio-frequency (*RF*) magnetic field pulse of 90º at a time $t_0 = 0$ and refocused by a 180º *RF* pulse. Representing the magnetic field gradients

$$G(t) = g \sum_{t_k = \{0, \delta, \delta+\Delta, \Delta\}} (-1)^{k-1} H(t - t_k) \qquad (4)$$

(here $H(t)$ is a Heaviside function) in the frequency domain, $\lim_{t\to\infty}\left(\int_0^t G(t')e^{i\omega t'}dt'\right)$, one can obtain the attenuation in the form:

$$\alpha(t) = \frac{\gamma^2 D}{2\pi} \int_{-\infty}^{\infty} S(\omega)\langle u(\omega)u^*(\omega)\rangle d\omega, \qquad (5)$$

with the gradient spectrum [28],

$$S(\omega) = \frac{g(\omega)g^*(\omega)}{\omega^2} \qquad (6a)$$

and analytic part of Fourier transform of magnetic gradients:

$$g(\omega) = ig\left(e^{-i\omega\delta} - 1 + e^{-i\omega\Delta}\left(1 - e^{-i\omega\delta}\right)\right). \qquad (6b)$$

If we insert Eq.(3) and Eq.(6) in Eq.(5) we obtain:

$$\alpha\left(\delta,\Delta,\tau\right)=-\frac{4g^2\gamma^2D}{\pi}\left(\mathrm{Re}\int_{-\infty}^{\infty}\frac{e^{i\omega\Delta}\sin^2\left(\omega\delta/2\right)d\omega}{\omega^2\left(\omega^2+2/\tau^2\right)}-\int_{-\infty}^{\infty}\frac{\sin^2\left(\omega\delta/2\right)d\omega}{\omega^2\left(\omega^2+2/\tau^2\right)}\right).\qquad(7)$$

Integral in Eq.(7) can be simplified in a limit of weak velocity autocorrelation using Taylor expansion:

$$\left.\frac{1}{\omega^4\left(1+2/\left(\omega\tau\right)^2\right)}\right|_{\omega\tau\gg1}\approx\frac{1}{\omega^4}\left(1-\frac{2}{\left(\omega\tau\right)^2}\right).\qquad(8)$$

Then analytical continuation of integral in Eq.(7) and application of residue theorem [28] for contour integrals yields:

$$\alpha\left(\delta,\Delta,\tau\right)=\gamma^2g^2D\times$$

$$\times\left(\delta^2\left(\Delta-\frac{\delta}{3}\right)+\frac{1}{3\tau^2}\left(\left(\Delta^3\delta^2+\Delta\delta^4/2\right)-\frac{\delta^5}{20}\right)\right).\qquad(9)$$

It is worth noting that the dynamic autocorrelation velocity introduced in Eq.(3)

indicates the non-Gaussian nature of diffusion. This statement is clearly confirmed by the second perturbative term of Eq.(9), where quasi-nonstationary diffusion coefficient is D/τ^2.

In the free motion regime, $\omega\tau\to\infty$, spin-bearing particle independent on background structure. Then Eq.(8) can be approximated by power law, ω^{-4}, and attenuation factor at echo time (*TE*) in Eqs.(1,2) gives

$$\alpha\left(\delta,\Delta\right)=\gamma^2\delta^2g^2D\left(\Delta-\delta/3\right)\qquad(10)$$

which corresponds to the classical Stejskal-Tanner result [29].

Hierarchical model of random composite.
In general case, a composite soft medium (Fig.1b, left) can be represented as a matrix (*1*) with embedded inhomogeneities (*2*) characterized by different properties (for example, diffusivities).

b

c
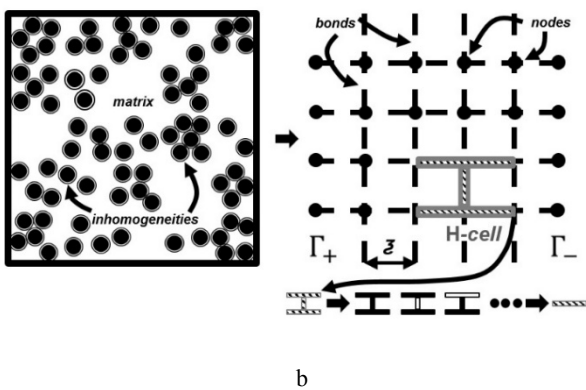
Figure 1.b – Heterogeneous material (composite) is modelled as a matrix (white color) with inclusions of random components (black disks). The composite can be divided into sections of scale z. It can be mapped on a lattice with different bond diffusion $\left\{D_1,D_2,...,D_k\right\}$ (right side of the figure). In the lattice, one can define a renormalization H-cell with its structural configurations.
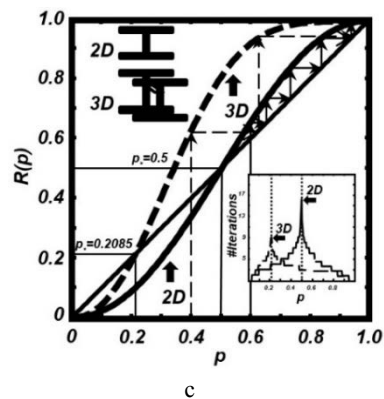
Figure 1.c – Renormalization curve, $R\left(p\right)$, for *2D* (solid line) and *3D* (dashed line) cases of coarse-grained H-cells (inner diagram). Unstable transformation points are indicated as p_*. The inner graph shows the number of recursive iterations of coarse-graining at the selected precision ε.
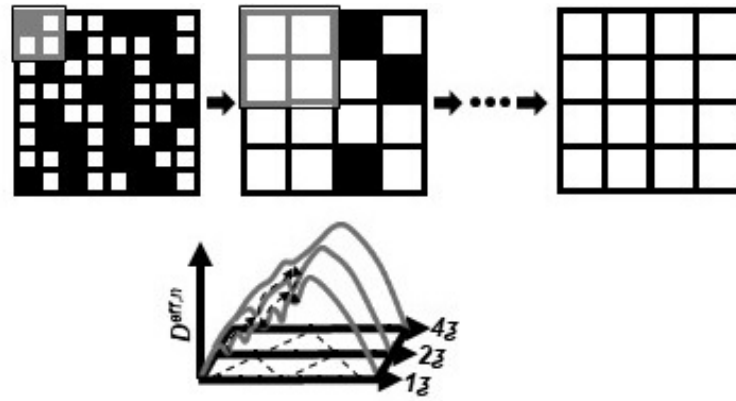
Figure 1.d – The effective diffusion value, $D^{eff,n}$, depends on the scale $\mathfrak{z}_n = n\mathfrak{z}$ (bottom of the figure) and can be modelled by renormalizing the H-cell in *2D* and *3D* Euclidean spaces. The coarse-graining procedure for the $\mathfrak{z}_n$ and $\mathfrak{z}_{n+1}$ scales is shown at the top of the figure.

We can assume the equilibrium of all flows of diffusing particles in the regime of fast movement at any place and time inside the composite. Then the discrete version of the law of conservation of mass looks like this:

$$\sum_{\substack{l \in S \backslash S_\Gamma \\ m \in S}}^{l \neq m} \Xi_{(lm)}\left(\psi_l - \psi_m\right) = 0, \qquad (11)$$

if ψ_l is a concentration of particles at l th node of the lattice (Fig.1b, right). The distribution of local diffusion properties, $\Xi_{(lm)}$, in Eq.(11) is governed by the binary function:

$$\Xi_{(lm)} = \Xi^{(1)}\delta_{(lm)} + \Xi^{(2)}\left(1 - \delta_{(lm)}\right), \qquad (12)$$

where all possible lattice configurations of the function in Eq.(12) are determined by the indicator $\delta_{(lm)} = \{0,1\}$ generating the set E. We map the composite to a lattice of S interior and S_Γ contact boundary Γ nodes using Eq.(11). The bond (lm) can correspond either to phase (*1*) or (*2*) with probabilities p and q (keeping $p + q = 1$) and characterized by properties $\Xi^{(1)}$ or $\Xi^{(2)}$. The Dirichlet boundary condition in Eq.(11) is given $\psi_m\big|_{\Gamma_+} = 0$ and $\psi_m\big|_{\Gamma_-} = 1$ on the left, Γ_+, and right, Γ_-, sides of the lattice respectively (Fig.1b, right). Using boundary conditions together with Eq.(11), we can calculate the equivalent diffusion value, $\left\langle F\left(\left\{\Xi_{(lm)}, p\right\}\right)\right\rangle$. Note that it is averaged over all realizations of Eq.(12) on the lattice.

We simulate the effective (i.e. global) characteristics of a composite with randomly distributed local properties according to the renormalisation group method in real space [30,31,33] with a chosen H-cell with a minimal size $\mathfrak{z}$ (Fig.1b, right).
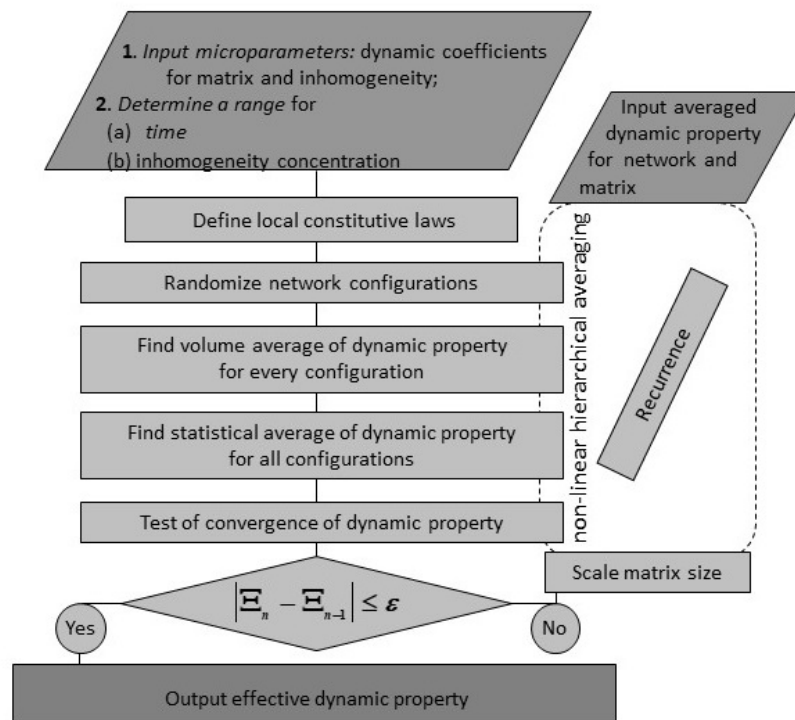
Figure 2 – Flowchart of coarse grinding procedure. There are three main components of the algorithm. These are preparation, recursive iterations and output of effective values.

The binary function of Eq.(12) in this case is an iterative transformation depending on the index n. Thus, the recursion for Eq.(12) is defined as

$$\begin{cases} \Xi_{(l'm'),n+1} = \left\langle F\left(\left\{\Xi_{(lm),n}, p_n\right\}\right)\right\rangle^{(1),n+1} \delta_{(l'm')} + \left\langle F\left(\left\{\Xi_{(lm),n}, q_n\right\}\right)\right\rangle^{(2),n+1} \left(1-\delta_{(l'm')}\right), \\ p_{n+1} = R\left(p_n\right) \end{cases} \tag{13}$$

where the equivalent diffusion function is separated into components $(k)=\{(1),(2)\}$ based on the connectivity of the bonds in the set E. Here the connectivity assumes the existence of a spanned cluster of inhomogeneities.

The transformation of p in Eq.(13) corresponds to the connectivity function $R(p)$ (Fig.1c) and can be expressed by polynomial equations

$$\left[\begin{array}{l} R(p)\big|_{2D} = p^5 + 5\left(1-p\right)p^4 + 8p^3\left(1-p\right)^2 + 2p^2\left(1-p\right)^3 \\ R(p)\big|_{3D} = p^{12} + 12p^{11}\left(1-p\right) + 66p^{10}\left(1-p\right)^2 + 220p^9\left(1-p\right)^3 + \\ \qquad + 493p^8\left(1-p\right)^4 + 776p^7\left(1-p\right)^5 + 856p^6\left(1-p\right)^6 + \\ \qquad + 616p^5\left(1-p\right)^7 + 238p^4\left(1-p\right)^8 + 48p^3\left(1-p\right)^9 + 4p^2\left(1-p\right)^{10} \end{array}\right. \tag{14}$$

characterized by unstable points $p_* = \{0.5_{2D}, 0.2085_{3D}\}$ [14] in *2D* and *3D* Euclidian dimensions. The size of spanned cluster at these points is maximal. The number of iterations for constructing a hierarchical lattice (Fig.1c, insert) is defined by the constraint $|p_n - p_{n+1}| \le \varepsilon$, where $\varepsilon > 0$ is an infinitely small number.

By virtue of this condition, the two components of the composite are indistinguishable after *l*-scale hierarchical averaging within $\mathit{z} << l << L$ (Fig.1d) which yields the convergence of binary properties to singular ones on the global scale L with effective properties matching component (*1*) or (*2*), according to the selection of the starting probability p_0 at the first iteration step $n = 0$.

The averaged equivalent value can be separated according to the connectivity of realizations in the set E at each iteration step of the coarse-graining algorithm presented in Fig.2. In Eq.(12) the initial

property at $n = 0$ is a diffusion factor in signal given in Eq.(9):

$$\Xi_{(lm),0} = \begin{bmatrix} D_{(1)}, & component\ (1) \\ D_{(2)}, & component\ (2) \end{bmatrix}, \quad (15)$$

which depends on the heterogeneous material properties.

Numerical simulation results.

The effective diffusion, $D^{eff} = \lim_{n \to \infty} \left(\Xi_{(lm),n} \right)$ (Eq.(13)), can be modelled if the initial values of the parameters are determined in Eq.(15). The simulation parameters can be found in Table 1. We assume a diffusion time Δ of about 5-30 ms and typical duration of diffusion weighting gradient, δ, was assigned as 6 ms. These parameters provide variation of widely acceptable attenuation factor [11], *b-value* $= \gamma^2 \delta^2 g^2 (\Delta - \delta/3)$, approximately from 100 ms/mm² till 1000 ms/mm².

**Table 1** – Parameters for numerical simulation of the effective diffusion signal.

	$D^{(1)}/D^{(2)}$	δ, ms	Δ, ms	p	τ, ms
2D/3D	*2*	*6*	*[5,30]*	*[0,1]*	*100*
2D/3D	*1.2*	*6*	*[5,30]*	*[0,1]*	*20*

To understand the main qualitative changes in the behavior of the diffusion signal, we selected correlation times inside and outside the diffusion time range (20 ms and 100 ms, respectively). This choice of parameter settings allows one to estimate the effective attenuation using Eqs. (13-15) and the procedure described in Fig. 2. It is worth noting that the scale of typical molecular propagation in this case is within a few micrometers, which determines the upper limit of applicability of the model.

First of all, consider the case of a long correlation time (100 ms). According to Eq.(9), the contribution of the term $\sim 1/\tau^2$ is negligible, and the damping occurs due to the usual Stejskal-Tanner (Eq. (10)). Indeed, in Fig.3a,b if $p \to 0$ and $p \to 1$ we observe a linear Stejskal-Tanner attenuation on a semi-logarithmic scale. The magnitude of the line slope

depends on the diffusion characteristics of the matrix (1) or heterogeneity (2). It is worth pointing that diffusion ratio, $D_{(1)}/D_{(2)}$, is close to 1 in this case and, as a consequence, increasing the concentration of inclusions changes the diffusion signal linearly at the large diffusion time. The same effect is observed for short diffusion times but with a lower rate.

If we reduce correlation time and make it short enough (20ms), then the signal changes nonlinearly with the diffusion time and linearly with the concentration of inclusions (Fig.3c,d). The rate of nonlinear dependency of the signal versus diffusion time is governed by correlation parameter according Eqs.(9,15). It should be pointed out, that in both cases, short and long correlation time, results were independent on unstable point p_* and the Euclidian dimension.
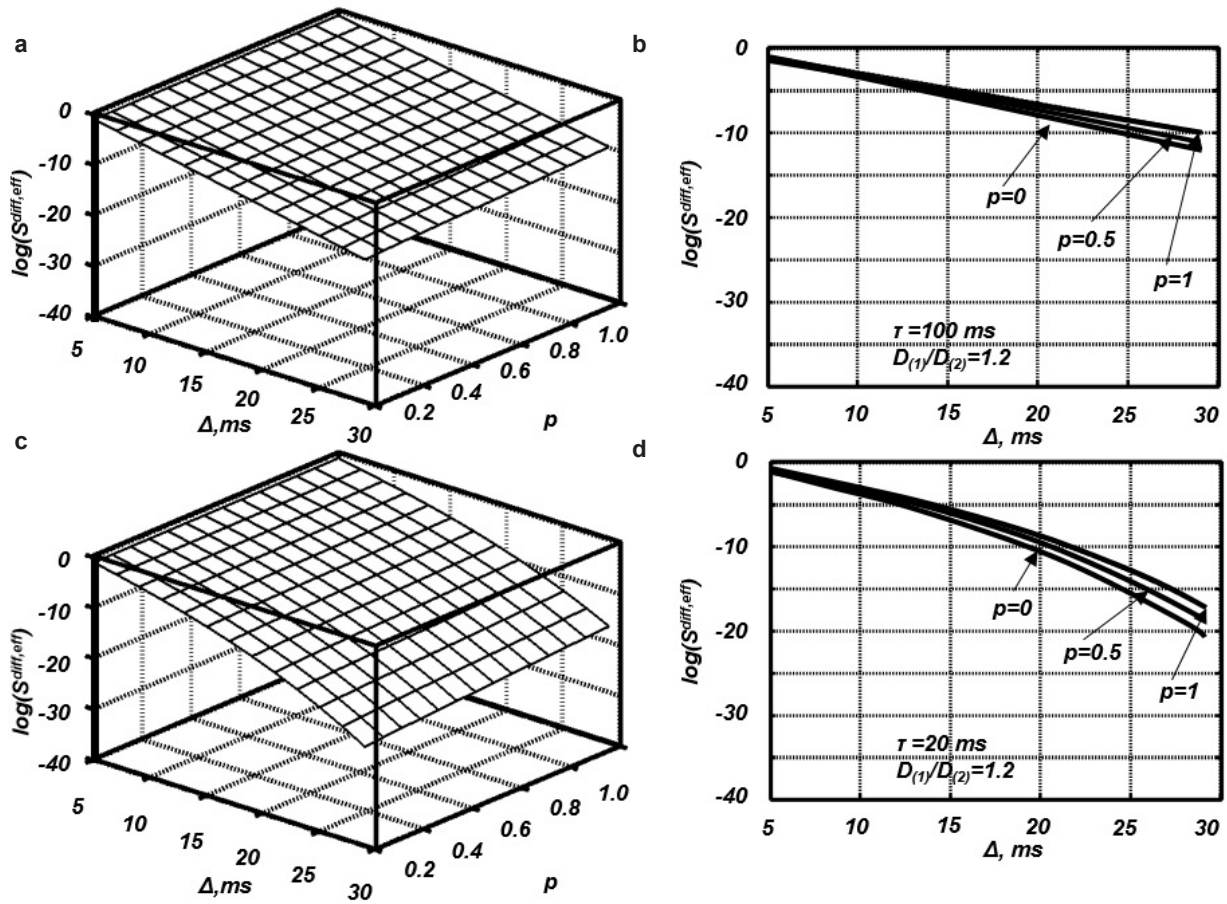
Figure 3 – Effective diffusion-weighted signal in *2D* and *3D* (**a-d**) cases as a function of diffusion time and inclusion concentration. There is no dependence on the Euclidean dimension and the signal changes linearly with increasing concentration of inclusions. The classical Stejskal-Tanner function is valid at high correlation times (**a, b**). Strong nonlinear dynamic effects are observed with reduced correlation time (**c,d**). Simulation results are presented on a semi-logarithmic scale.

The situation changes qualitatively if we increase the ratio $D_{(1)}/D_{(2)}$. If the correlation time is long (100 ms), then nonlinear time-dependent effects are invisible. In this case, we observe the dependence of the Stejskal-Tanner signal on the diffusion time. An increase in the concentration of inclusions leads to a nonlinear increase in the signal, which is clearly observed at long diffusion times (Fig. 4a,b). Near percolation threshold, p_*, we observe a jump of the signal. The value of the jump depends on the ratio $D_{(1)}/D_{(2)}$. Since the location of the percolation threshold is a function of the Euclidean dimension, the jump region of about 0.5 in *2D* shifts to 0.2085 in *3D* (Fig. 4a,b).

Shortening of the correlation time (20ms) leads to the pronounced nonlinear effects for a signal as a function of diffusion time (Fig.4c,d). In addition to

this increase of the concentration of inclusions sets percolation jump which is located differently for *2D* and *3D* Euclidean cases. The observed situation, when $D_{(1)}/D_{(2)}$ is large, can be explained by the length of molecule propagation. For example, at $p_* + \varepsilon$ the spanned cluster of network with a high diffusivity is built, which significantly regulates the molecule propagation distance. The strongest nonlinearity in the location of the unstable point degenerates with increase of network concentration. Thus nonlinearity can be characterized by two nearly linear modes before and after the unstable points (see line segments in Fig.4c,d). The modes at high diffusion time depends on the Euclidian dimension and are asymmetrical in *3D*. In *3D* case additional degree of freedom reduces a probability of the cluster self-crossing which influences on spanned cluster topology. In *2D* case spanned cluster resembles

network and in *3D* case spanned cluster is a backbone with many branches. Thus, nonlinearity in p_* reflects the cluster structure of the inclusion network. If cluster connectivity occurs for the first time, the nonlinearity of the diffusion properties takes on a maximum degree.
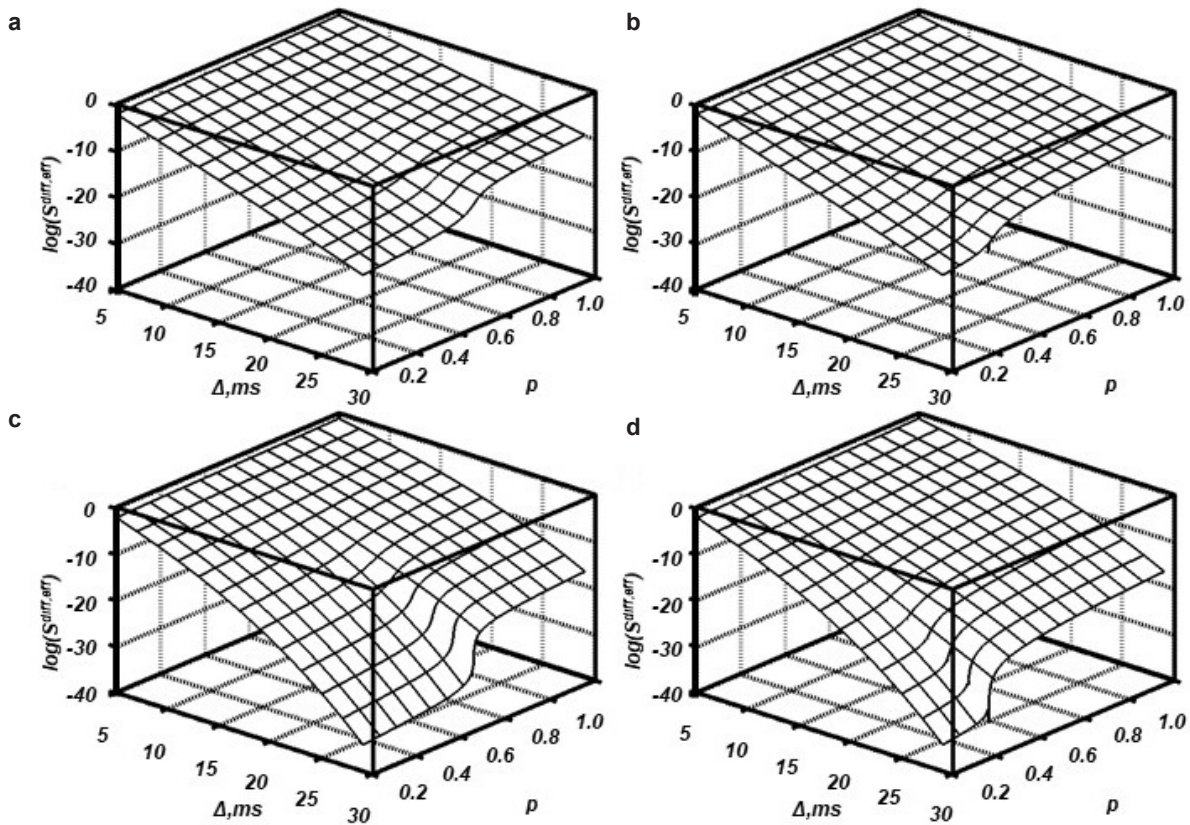
Figure 4 – Effective diffusion-weighted signal in *2D* (**a, c**) and *3D* (**b, d**) cases depending on the diffusion time and inclusion concentration. Near unstable points, nonlinear effects manifest themselves clearly and depend on the Euclidean dimension. The simulation results are presented on a semi-logarithmic scale.

Discussion and conclusion

Diffusion processes are very difficult to characterize, but they are of great interest in various fields of physics, medicine and biology. In this paper, we developed an effective medium framework for interpreting the diffusion-weighted MR signal and utilized the diffusion of spin-bearing molecules to probe the structural heterogeneity of the medium. Molecules diffuse through the medium and probe morphological information while moving in a fast limit regime. We introduced a basic dispersion characteristic – a molecular spin decay function with a hierarchy that includes all the diffusion properties of a random composite. Such a model simplifies an inherently complex problem to an ensemble of spatially distributed diffusions that determine MR

signal, which can be characterized by the scale symmetry of the medium. This approximation is useful because the structure explored by spin-carrying molecules remains close to a chaotic, as in the expected realistic conditions.

To solve the complex problem using an adequate mathematical apparatus, we have related the renormalisation group transformation to a diffusion-weighted time-dependent signal. It is demonstrated that the effective medium approximation describing inhomogeneous diffusion leads to a time-dependent switching of the diffusion in the neighborhood of the point of highest disorder. However, this switching qualitatively differs for different Euclidean dimensions. In particular, the quantitative jump occurs earlier for *3D* and later for *2D* cases. We also discussed a limitation of the model, indicating that in

the case of large spatial variations of the internal magnetic field gradients compared to the diffusion scale, the contamination of molecular motion can lead to the loss of information on its distribution.

In general, we have shown that important parameters of a complex medium are the dispersion of local diffusion and the concentration of its components, as well as different length scales in the spatial distribution of diffusion. The proposed approach is a powerful additional tool for theoretical interpretation of experimental data obtained for meta- and natural materials.

Appendix I: The scale of the phase autocorrelation effect.

Spin-phase growth due to molecular Brownian motion in the presence of linear magnetic field can be described as an additive discrete function within repetitive Bernoulli scheme of trials with linearly increasing value of random variable [1]. The analytical form of probability density function is ultimately close to normal, $\aleph\left(0,\left\langle \varphi^2 \right\rangle\right)$, according central limit theorem, and experimentally observable mean can be calculated if spin is represented as a phasor:

$$\left\langle e^{i\varphi t} \right\rangle = \lim_{t \to 1} \int_{-\pi}^{\pi} e^{i\varphi t} \aleph\left(0,\left\langle \varphi^2 \right\rangle\right) d\varphi . \quad \text{(AI,1)}$$

We can estimate the phase change due to molecular single jump $\Delta\varphi = \tilde{\gamma} g \Delta x \Delta t$, if magnetic field gradient $g = 25 \cdot 10^{-3} \left[T/m \right]$, gyromagnetic ratio $\tilde{\gamma} = 267.5 \cdot 10^6 \left[rad/(T \cdot s) \right]$, and molecular jump length $\Delta x = 2.5 \cdot 10^{-10} \left[m \right]$, which occurs

within time interval $\Delta t = 10^{-14} \left[s \right]$ [34]. The typical experiment duration is $\delta = 2 \cdot 10^{-2} \left[s \right]$ and molecular diffusion $D = 2.3 \cdot 10^{-9} \left[m^2/s \right]$ at temperature $25^0 C$. In this case spin obtains a phase $\Delta\varphi = 1.7 \cdot 10^{-17} \left[rad \right]$ after a single jump. During time of experiment the total number of jumps, N, is $2 \cdot 10^{12}$ providing the phase change, and, as a consequence, correlation effect, $0.91 < \pi$. This estimation allows to introduce improper integral with a high precision and estimate it as a Fourier-transform of a normal distribution:

$$\lim_{t \to 1} \int_{-\infty}^{\infty} e^{i\varphi t} \aleph\left(0,\left\langle \varphi^2 \right\rangle\right) d\varphi = e^{-\frac{\left\langle \varphi^2 \right\rangle}{2}} \quad \text{(AI,2)}$$

with $\left\langle \varphi^2 \right\rangle/2 = \alpha(t)$ according Eq.(1).

Appendix II: Calculation of MR signal attenuation in the presence of background gradients.

Modern MR scanners are equipped with active-resistive shimming coils to reduce small imperfections in the main magnetic field, B_0, and susceptibility effects. In this Appendix, we extend Eq.(9) to the case of linear background gradients with amplitude, g_s (Fig. 1), assessing the impact of the shimming procedure. This result is important when working with MR scanners, where residual gradients are not optimally shimmed, but in well shimmed systems the additional terms associated with g_s can be neglected. To calculate the attenuation, we use Eq. (5) with a modified $g(\omega)$:

$$g(\omega) = i \begin{pmatrix} -g_s \left(1 - e^{-i\omega t_1}\right) - \left(g_s + g\right) e^{-i\omega t_1} \left(1 - e^{-i\omega \delta}\right) - g_s e^{-i\omega(t_1 + \delta)} \left(1 - e^{-i\omega t_2}\right) + \\ g_s e^{-i\omega \Delta} \left(1 - e^{-i\omega t_1}\right) + \left(g_s + g\right) e^{-i\omega(\Delta + t_1)} \left(1 - e^{-i\omega \delta}\right) + g_s e^{-i\omega(\Delta + t_1 + \delta)} \left(1 - e^{-i\omega t_2}\right) \end{pmatrix} \quad \text{(AII,1)}$$

with t_1 being the delay between 90º *RF* excitation pulse and the start of the first gradient pulse and t_2 being the delay between the end of the second gradient and the center of the echo.

The integral in Eq.(5) with the new $g(\omega)$ (Eq.(AII,1)) can be calculated after analytical continuation on the complex plane and application of the residue theorem [28]:

$$\alpha\left(\delta,\Delta,t_1,t_2\right)\big/\gamma^2 D = \left(g+g_s\right)^2 \delta^2\left(\Delta-\delta/3\right)+$$

$$\frac{g_s^2}{6}\left(\begin{array}{c}\displaystyle\sum_{a_k=\{t_1,0,t_2,t_1+t_2\}}\left(-1\right)^{k+1}\left(\delta-\Delta+a_k\right)^3 + \sum_{a_k=\{t_1,t_1+t_2,t_2\}}2\left(-1\right)^{k+1}\left(\delta+a_k\right)^3 - \sum_{a_k=\{\delta,t_1,t_2,2^{1/3}\Delta\}}2a_k{}^3 + \\[2ex] \displaystyle\sum_{a_k=\{\delta,t_1,t_2\}}\left(\Delta+a_k\right)^3 + \sum_{a_k=\{t_1,t_2\}}\left(\Delta-a_k\right)^3 + \sum_{a_k=\{t_1,t_1+t_2,t_2\}}\left(-1\right)^{k}\left(\delta+\Delta+a_k\right)^3\end{array}\right)-$$

$$\frac{\left(g+g_s\right)g_s}{6}\left(\begin{array}{c}\displaystyle\sum_{a_k=\{t_1,0,t_2,0\}}\left(-1\right)^{k+1}\left(\delta-\Delta+a_k\right)^3 + \sum_{a_k=\{t_1,\delta,t_2,\delta\}}\left(\Delta+a_k\right)^3 + \sum_{a_k=\{t_1,t_2\}}2\left(\delta+a_k\right)^3 + \\[2ex] \displaystyle\sum_{a_k=\{t_1,t_2\}}\left(\Delta-a_k\right)^3 + \sum_{a_k=\{t_1,t_2\}}\left(\Delta+\delta+a_k\right)^3 - \sum_{a_k=\{\Delta,\delta,2^{-1/3}t_1,2^{-1/3}t_2\}}4a_k{}^3\end{array}\right) \quad \text{(AII,2)}$$

The correctness of Eq.(AII,2) can be checked by posing $t_1=t_2$ and $g_s=g$ obtaining Eq.(10) with a changed amplitude and duration of the gradient. In the general case, the gradients g_s and g may not coincide, which leads to the absolute value of the vector summation of these gradients in Eq.(AII,2).

In the case of a disturbance with weak correlation, Eq.(AII,2) includes an additional term:

$$\alpha\left(\delta,\Delta,\tau,t_1,t_2\right)\big/\gamma^2 D = \alpha\left(\delta,\Delta,t_1,t_2\right)\big/\gamma^2 D - \frac{\left(g+g_s\right)^2}{60\tau^2}\left(\delta^5 - \sum_{a_k=\{-\delta,0,\delta,0\}}\left(-1\right)^{k+1}\left(\Delta+a_k\right)^5\right)+$$

$$\frac{g_s^2}{60\tau^2}\left(\begin{array}{c}\displaystyle\sum_{a_k=\{t_1,0,t_2,t_1+t_2\}}\left(-1\right)^{k+1}\left(\delta-\Delta+a_k\right)^5 + \sum_{a_k=\{t_1,t_1+t_2,t_2\}}2\left(-1\right)^{k+1}\left(\delta+a_k\right)^5 - \sum_{a_k=\left\{\delta,t_1,t_2,\atop 2^{1/3}\Delta\right\}}2a_k{}^5 + \\[2ex] \displaystyle\sum_{a_k=\{\delta,t_1,t_2\}}\left(\Delta+a_k\right)^5 + \sum_{a_k=\{t_1,t_2\}}\left(\Delta-a_k\right)^5 + \sum_{a_k=\{t_1,t_1+t_2,t_2\}}\left(-1\right)^{k}\left(\delta+\Delta+a_k\right)^5\end{array}\right)-$$

$$\frac{\left(g+g_s\right)g_s}{60\tau^2}\left(\begin{array}{c}\displaystyle\sum_{a_k=\{t_1,0,t_2,0\}}\left(-1\right)^{k+1}\left(\delta-\Delta+a_k\right)^5 + \sum_{a_k=\{t_1,\delta,t_2,\delta\}}\left(\Delta+a_k\right)^5 + \sum_{a_k=\{t_1,t_2\}}2\left(\delta+a_k\right)^5 + \\[2ex] \displaystyle\sum_{a_k=\{t_1,t_2\}}\left(\Delta-a_k\right)^5 + \sum_{a_k=\{t_1,t_2\}}\left(\Delta+\delta+a_k\right)^5 - \sum_{a_k=\{\Delta,\delta,2^{-1/3}t_1,2^{-1/3}t_2\}}4a_k{}^5\end{array}\right) \quad \text{(AII,3)}$$

Eq.(AII,3) can be verified by setting $t_1=t_2$ and $g_s=g$ to obtain Eq. (9).

References

1. Callaghan P. *Principles of Nuclear Magnetic Resonance Microscopy.* Oxford University Press, 1994.
2. Novikov D.S.et al. Random walks with barriers, *Nature Physics.* 7(6) (2011) 508-514.
3. Ernst M. H. et al. Long time tails in stationary random media, *Journal of statistical physics.* 34 (3/4) (1984) 477-495.
4. Novikov D.S. et al. Revealing mesoscopic structural universality with diffusion, *Proceedings of the National Academy of Sciences.* 111 (14) (2014) 5088-5093.
5. Novikov D.S. et al. Effects of mesoscopic susceptibility and transverse relaxation on diffusion NMR, *Journal of magnetic resonance.* 293 (2018) 134-144.
6. Stauffer D. Scaling theory of percolation clusters, *Physics Reports.* 54 (1) (1979) 1-74.
7. Stanley H.E. *Introductions to Phase Transitions and Critical Phenomena.* Oxford University Press, 1971.
8. Dykhne A., Snarski A., Zhenirovski M. Stability and chaos in randomly inhomogeneous two-dimensional media and LC circuits, *Physics: Uspekhi.* 47 (8) (2004) 821-828.

9. Posnansky O. Effective diffusion in random composites measured by NMR, *Journal of magnetism and magnetic materials*. 466 (2018) 92-105.

10. Novikov V.V., Zubkov D.Y. Conductivity in a magnetic field of a three-dimensional composite with a random fractal structure, *Phys. Rev. B*. 73 (2006) 054202.

11. Wisniowski R., Olchawa W., Fraczek D., Piasecki R. On multi-scale percolation behaviour of the effective conductivity for the lattice model with interacting particles, *Physica A*. 444 (2016) 799-807.

12. Posnansky O., Huang R., Shah N. The truncated Levy-flight process: Application to the random spin phase change in non-linear magnetic fields, *Physica A: Stat. Mech. and its Applications*. 370 (2) (2006) 553-564.

13. Bloembergen N., Purcell E.M., Pound R.V. Relaxation effects in nuclear magnetic resonance absorption, *Phys. Rev.* 73 (1948) 679.

14. Posnansky O. Tensor of effective susceptibility in random magnetic composites: application to two-dimensional and three-dimensional cases, *Journal of molecular structure*. 1160 (2018) 293-303.

15. Shklovskii B.I., Efros A.L. *Electronic Properties of Doped Semiconductors, Springer Series in Solid State Sciences*. Springer-Verlag, 1984.

16. Reynolds P. J., Klein W., Stanley H. E. Large-cell Monte-Carlo renormalization group for percolation, *Phys. Rev. B*. 21 (1980) 1223.

17. Bergman D. J., Stroud D. G. High-field magnetotransport in composite conductors: Effective-medium approximation, Phys. Rev. B. 62 (2000) 6603.

18. Barabash S. V., Bergman D. J., Stroud D. G. Magnetoresistance of three-constituent composites: Percolation near a critical line, *Phys. Rev. B*. 64 (2001) 174419.

19. Bernasconi J., Real-space renormalization of bond-disordered conductance lattices, *Phys. Rev. B* 18(5) (1978) 2185.

20. Marinari E., Parisi G., Ruelle D., Windey P. Random walk in a random environment and 1=f noise, *Phys. Rev. Lett. 50* (1983) 1223.

21. Bouchaud J.-P., Georges A. Anomalous diffusion in disordered media: Statistical mechanisms, models and physical applications, *Phys. Rep.* 195 (1990) 127-293.

22. Haus J. W., Kehr K. W. Diffusion in regular and disordered lattices, *Phys. Rep.* 150 (1987) 263-406.

23. Posnansky O. Dynamic characteristics of the effective susceptibility function in random three-component system, *Physica A: Stat. Mech. and its Applications*. 473 (2017) 18-28.

24. Posnansky O. Viscoelastic properties of a hierarchical model of soft biological tissue: two-dimensional and three-dimensional cases, *Journal of Statistical Physics*, 164 (5) (2016) 1043-1061.

25. Posnansky O. On the influence of microscopic architecture elements to the global viscoelastic properties of soft biological tissue, *Physica D*. 289 (2014) 1-11.

26. Slichter Ch. P. *Principles of Magnetic Resonance*. Harper & Row Inc., 1963.

27. Stepisnik J. NMR measurement and Brownian movement in the short-time limit, *Physica B*. 198 (1994) 299-306.

28. Arfken G. B., Weber H. J. *Mathematical Methods for Physicist* (6th ed.). Elsevier Academic Press, 2005.

29. Stejskal E. O., Tanner J. E. Spin Diffusion Measurements: Spin Echoes in the Presence of a Time Dependent Field Gradient, *Journal of Chemical Physics*. 42 (1965) 288-292.

30. Uhlenbeck G.E., Ornstein L.S. On the Theory of the Brownian Motion, *Phys. Rev.* 36 (1930) 823.

31. Reynolds P. J., Klein W., Stanley H. E. A real-space renormalization group for site and bond percolation, *Journal of Physics C: Solid State Physics*. 10 (8) (1977) L167.

32. Posnansky O., Kupriyanova Y., Shah N.J. On the problem of gradient calibration in diffusion weighted imaging, *International Journal of Imaging Systems and Technology*. 21 (3) (2011) 271-279.

33. Posnansky O., Shah N.J. On the problem of diffusivity in heterogeneous biological materials with random structure, *Journal of Biological Physics*. 34 (6) (2008) 551-567.

34. feynmanlectures.caltech.edu

Information about author:
Posnansky Oleg P. – PhD, scientific researcher, BIF-IZKF, RWTH Aachen University, Aachen, Germany, e-mail: opoznans@gmail.com